Meteoritics & Planetary Science 1–13 (2024)
doi: 10.1111/maps.14266

Report

Bidirectional reflectance distribution function measurements of characterized Apollo regolith samples using the visible oxford space environment goniometer

R. J. CURTIS[1]*, T. J. WARREN[1], K. A. SHIRLEY[1], D. A. PAIGE[2], and N. E. BOWLES[1]

[1]Atmospheric, Oceanic and Planetary Physics, Department of Physics, University of Oxford, Oxford, UK
[2]Department of Earth and Space Sciences, University of California, Los Angeles, California, USA

*Correspondence
R. J. Curtis, Atmospheric, Oceanic and Planetary Physics, Department of Physics, University of Oxford, Oxford OX1 44BH, UK.
Email: rowan.curtis@physics.ox.ac.uk

(*Received 18 June 2024; revision accepted 29 August 2024*)

Abstract–A laboratory study was performed using the Visible Oxford Space Environment Goniometer in which the broadband (350–1250 nm) bidirectional reflectance distribution functions (BRDFs) of two representative Apollo regolith samples were measured, for two surface roughness profiles, across a range of viewing angles—reflectance: 0–70°, in steps of 5°; incidence: 15°, 30°, 45°, and 60°; and azimuthal: 0°, 45°, 90°, 135°, and 180°. The BRDF datasets were fitted using the Hapke BRDF model to (1) provide a method of comparison to other photometric studies of the lunar regolith and (2) to produce Hapke parameter values which can be used to extrapolate the BRDF to all angles. Importantly, the surface profiles of the samples were characterized using an Alicona 3D® instrument, allowing two of the free parameters within the Hapke model, φ and $\overline{\theta}$, which represent porosity and surface roughness, respectively, to be constrained. The study determined that, for $\overline{\theta}$, the 500–1000 μm size-scale is the most relevant for the BRDF. Thus, it deduced the following "best fit" Hapke parameters for each of the samples: Apollo 11 rough—$w = 0.315 \pm 0.021$, $b = 0.261 \pm 0.007$, and $h_S = 0.039 \pm 0.005$ (with $\overline{\theta} = 21.28°$ and $\varphi = 0.41 \pm 0.02$); Apollo 11 smooth—$w = 0.281 \pm 0.028$, $b = 0.238 \pm 0.008$, and $h_S = 0.032 \pm 0.006$ (with $\overline{\theta} = 13.80°$ and $\varphi = 0.60 \pm 0.02$); Apollo 16 rough—$w = 0.485 \pm 0.155$, $b = 0.155 \pm 0.083$, and $h_S = 0.135 \pm 0.007$ (with $\overline{\theta} = 21.69°$ and $\varphi = 0.55 \pm 0.02$); Apollo 16 smooth—$w = 0.388 \pm 0.057$, $b = 0.063 \pm 0.033$, and $h_S = 0.221 \pm 0.011$ (with $\overline{\theta} = 14.27°$ and $\varphi = 0.40 \pm 0.02$). Finally, updated hemispheric albedo functions were determined for the samples, which can be used to set laboratory measured visible scattering functions within thermal models.

INTRODUCTION AND MOTIVATION

Lunar Photometry

Understanding how the surfaces of airless planetary bodies, such as the Moon, scatter visible light enables constraints to be placed on their surface properties and top boundary layer inputs to be set within thermal models, such as the advanced thermophysical model (ATPM) and the Oxford 3D thermal model (O3DTM; King et al., 2019; Rozitis & Green, 2011). This scattering behavior can be described by a BRDF. Initially, within thermal models, scattering functions, for example, BRDFs, for the lunar regolith were assumed to be Lambertian (i.e., the same in all directions with a cosine drop-off) or were set using measurements at a limited range of viewing angles. Recent goniometry studies such as Foote et al. (2020) and Curtis, Warren and Bowles (2021a) have demonstrated the need for more accurate laboratory measured visible scattering functions

by measuring non-Lambertian initial reference photometry data sets for representative lunar regolith samples.

To be able to interpret BRDF data in terms of a planetary body's physical and compositional properties, we need (1) an appropriate photometric model and (2) a set of reference laboratory photometric measurements for returned samples or, in their absence, for well-characterized and comparable simulant samples. Over the past five decades, the Hapke bidirectional reflectance distribution function (BRDF) model has been developed (Hapke, 1981, 1984, 1986, 2002, 2008, 2012, 2021; Hapke et al., 1998), which has become the standard photometric model in planetary science because (1) it has been extensively validated using laboratory and remote sensing studies and (2) it contains nine free parameters which relate to the compositional and physical properties of the surface (for a more detailed description of the Hapke BRDF model, see Hapke, 2012 and Part 2.3).

Since the Hapke model was first described, various goniometer systems have measured BRDFs for a range of particulate samples such as regolith simulants (Gunderson et al., 2006), regolith/ice mixtures (Yoldi et al., 2015), and terrestrial analog materials and meteorites (Curtis et al., 2023; King et al., 2022; Potin et al., 2018). These include studies made using the Physikalisches Institut Radiometer Experiments (PHIRE-1 and PHIRE-2) (Gunderson et al., 2006), the SHADOWS spectro-gonio radiometer (Potin et al., 2018), the Blacklab goniometer system (Biggar et al., 2003), and the Visible Oxford Space Environment Goniometer (VOSEG) (Curtis et al., 2023; King et al., 2022). In 2010, Foote et al. measured BRDFs of the same Apollo 11 (mare) and 16 (highlands) regolith samples used in this study, using the Bloomsburg University Goniometer (BUG) (Foote et al., 2010; Johnson, 2008). The study concluded by suggesting that further BRDF measurements of Apollo regolith samples were required to deconvolve the influence of porosity on the measured BRDFs of the samples. Within their publications Hapke (2012), Shepard and Helfenstein (2007), and Foote et al. (2020), all suggest additional goniometry measurements are required to further test the Hapke model and to further study how physical properties such as porosity and surface roughness influence visible light scattering for planetary regolith and simulant samples (Foote et al., 2020).

In this study, the VOSEG (Curtis, Warren, & Bowles, 2021b) was used to measure a suite of BRDFs in the principal (azimuthal angle = 0/180°), out-of-principal (azimuthal angle = 90/270°), and diagonal (azimuthal angle = 45/135°) planes for two representative Apollo lunar regolith samples, 10084 (Mare) and 68810 (Highlands), with two surface roughness profiles (e.g., smooth and rough). The samples measured in the study were characterized using an Alicona 3D® non-contact surface profiler before the BRDF suite was measured. Hence, filling factor, φ, and root-mean-square (RMS) slope angle values (across 10–1000 μm size scales) could be determined for the samples. The Hapke BRDF model was fitted to the data set, leading to the determination of Hapke parameters w, b, and h_S for the rough and smooth samples. These parameters shed light on the surface properties and compositional nature of the lunar regolith, allow constraints to be placed on the size-scale of $\overline{\theta}$ within the Hapke Model, and can be used to derive accurate scattering function inputs within thermal model, such as the O3DTM. Furthermore, they can be compared to Hapke parameters determined in previous laboratory and remote sensing studies of the lunar regolith, such as Foote et al. (2020) and Sato et al. (2014).

Apollo Regolith Samples

The curation and analysis team for extraterrestrial materials (CAPTEM) provided two representative lunar regolith samples. The Apollo 11 sample, 10084, was collected at (23.47242165E, 0.673705459N) and is representative of low albedo lunar mare regolith. It is primarily basaltic, but contains a substantial non-mare component. The sample consists of ~66% crystalline mare basalt; ~20% feldspathic particles from the lunar highlands; ~8% potassium, rare earth elements, and phosphorous (KREEP)-bearing, impact melt breccias; 5% orange volcanic glass; and 1% meteoritic material (Foote et al., 2020; Morris, 1983), and all particles are <1 mm. For a comprehensive description of 10084, see Meyer (2009).

The Apollo 16 sample, 68810, is a < 1 mm residue sample from ~(15.48301029 E, −8.974000931 N) and is representative of high albedo lunar highlands regolith. It has not yet been characterized in terms of composition, but is expected to primarily consist of impact breccias and anorthositic rocks (Foote et al., 2020; Morris, 1983).

EXPERIMENTAL METHODS

Sample Preparation and Surface Profiling

For each of the Apollo samples, two samples were prepared with different levels of surface roughness. The first set of "smooth" samples was prepared by spooning regolith into the sample cups and then the surfaces were smoothed over using the edge of a metal blade. For the second, "rough" set of samples, the regolith was sprinkled into the sample cups to produce a rougher

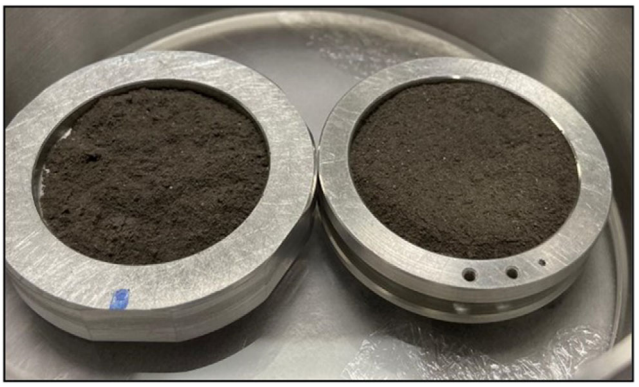

FIGURE 1. Left: A "rough" Apollo 16 (68810) sample used in the VOSEG physical property variation study. Right: A "smooth" Apollo 16 (68810) sample used in the VOSEG physical property variation study.

surface (an investigation into the repeatability of this process when repacking the sample is detailed in the supplementary materials). Examples of smooth and rough 68810 samples are shown in Figure 1.

Surface profiles of the samples were captured using an Alicona® 3D instrument, with a lateral spatial resolution of 10 μm. A 3-D color representation of the imaged surface of the rough Apollo 16 (68810) sample, with 10 μm lateral resolution and 1 μm vertical resolution, is shown in Figure 2.

The RMS slope angle values were calculated at 10, 50, 100, 500, and 1000 μm resolutions (see Table 1). In addition to the RMS slope angle values, the filling factors of the samples were determined. This was done by measuring the sample's depth from the top of the sample cup using the Alicona 3D®. The sample cup has a known depth of 3 mm, allowing bulk density, and hence filling factor to be calculated for the sample. Filling factors were calculated as in Foote et al. (2020) and Sato et al. (2014), by dividing the bulk density value by the average density of an average Apollo regolith particle of 3100 kg m^{-3}.

For a more detailed description of the surface profiling process, see the supplementary materials.

The size scale (or length-scale) refers to the spatial resolution used when calculating the RMS slope angle. For instance, a 10 μm size scale implies that RMS slope angles were calculated between points on the image which have a distance between them of 10 μm. Using a larger size scale (i.e., 1000 μm, as opposed to 10 μm) will naturally lead to lower values in RMS slope angle, as smaller scale topography variations will not be accounted for. This is demonstrated in Figure 3, which shows the RMS slope angle values measured for this study's Apollo samples across a range of size scales, and measurements of the lunar regolith at the lunar surface. The surface roughness of the lunar regolith at the lunar surface at various size-scales (0.085–85 mm) was studied in Helfenstein and Shepard (1999) using stereophotogrammetry images taken during the Apollo missions. How the RMS slope angles for the samples used in this study compare to those measured in Helfenstein and Shepard (1999) at the lunar surface is shown in Figure 3.

Figure 3 demonstrates how the surface roughness profiles of our samples are representative of what was observed at the lunar surface for the Apollo regolith surfaces imaged in Helfenstein and Shepard (1999).

Photometric Measurements

The VOSEG is an automated laboratory setup which can measure visible wavelength BRDFs in ambient conditions over a range of viewing angles (0–60° incidence, 0–70° reflectance, ~4–130° phase, 0–360° azimuthal). White Spectralon measurements taken by VOSEG agree (within the SE) with those taken by BUG —the goniometer system which was used to measure Apollo regolith samples in the Foote et al.'s (2020) study (Labsphere, 2017). VOSEG can measure down to ~4° phase angles—which means it can measure part of the opposition effect—and it can take measurements over a range of angles, up to and including 60° incidence and 70° reflectance angles. The VOSEG setup is shown in Figure 4 and is described in detail in Curtis, Warren, and Bowles (2021a).

The light reflected/scattered from the sample is measured using a visible-λ photodiode detector (RS Components-BPW21R), and the output signal is demodulated from the chopper reference signal using a lock-in amplifier (SR830-Stanford Research Systems). The output is then recorded on a PC. For each viewing angle, three measurements are made, and these values are averaged to produce a reflectance value relative to the White Spectralon® calibration target, which has a known and well-characterized reflectance function (Labsphere, 2017). The uncertainty in each reflectance value is calculated as the standard deviation of the three measurements. BRDFs can be calculated from reflectance values via the relation given in Equation (1):

$$\mathrm{BRDF}(\theta_r, \theta_i, \theta_a) = \frac{r_R(\theta_r, \theta_i, \theta_a)}{\cos(\theta_i)} \tag{1}$$

where $r_R(\theta_r, \theta_i, \theta_a)$ is the reflectance of the surface—that is, the ratio of scattered radiance at the detector to the collimated incident irradiance illuminating the surface—which is dependent on reflectance angle, θ_r; incidence angle, θ_i; and azimuthal angle, θ_a.

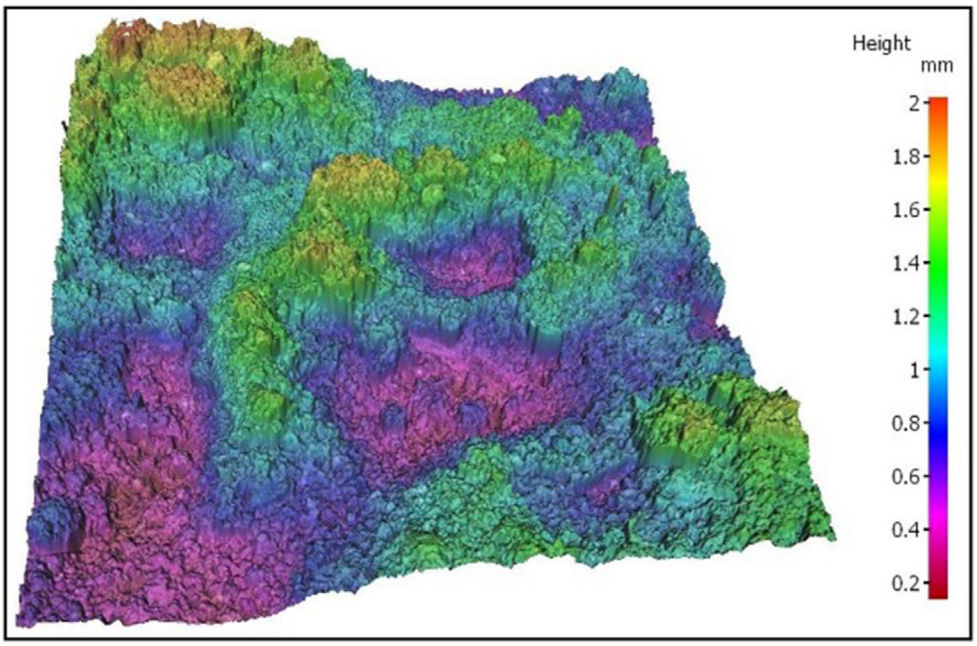

FIGURE 2. A 3-D surface profile taken by the Alicona 3D® for a roughly prepared surface of Apollo 16 (68810) highlands lunar regolith, with 10 μm lateral resolution and 1 μm vertical resolution. The RMS slope angles for this 10 × 10 mm part of the sample were determined to be 37.73° at 10 μm size-scale, 36.45° at 50 μm size-scale, 32.10° at 100 μm size-scale, 21.69° at 500 μm size-scale, 20.17° at 1000 μm size-scale.

TABLE 1. The filling factors, masses, and RMS slope angle values measured for the Apollo 11 (10084) and Apollo 16 (68810) rough and smooth samples measured in the VOSEG BRDF study. RMS slope angle values are given for the 10, 50, 100, 500, and 1000 μm size-scales.

Sample ➔	10084 Rough	10084 Smooth	68810 Rough	68810 Smooth	68810 Rough (#2)	68810 Smooth (#2)
φ ➔	0.41 ± 0.02	0.60 ± 0.02	0.40 ± 0.02	0.55 ± 0.02	0.39 ± 0.01	0.57 ± 0.02
Mass (kg)	0.0045	0.0048	0.0041	0.0043	0.0040	0.0046
Size-scale (μm)	RMS slope angle (°)					
10	41.036	33.456	37.732	34.539	37.755	33.205
50	40.660	30.571	36.452	32.491	36.607	30.170
100	36.153	24.637	32.097	27.106	32.118	24.034
500	21.283	13.805	21.693	14.271	21.199	12.269
1000	17.338	11.779	20.170	11.799	18.661	10.184

The Hapke BRDF Model

The reflectance of a particulate surface (assuming no effects from surface roughness), $r(\theta_r, \theta_i, \theta_a)$, can be predicted in relation to compositional and physical properties using Equation (2), from Hapke (2012):

$$r(\theta_r,\theta_i,\theta_a) = K\frac{w}{4\pi}\frac{\mu_r}{\mu_0+1}p(\theta_p)\ldots \left\{\left[1+B_{S0}B_S(\theta_p)\right]+\left[H\left(\frac{\mu_0}{K}\right)H\left(\frac{\mu_r}{K}\right)-1\right]\right\}\ldots \left[1+B_{C0}B_C(\theta_p)\right] \quad (2)$$

where K is porosity coefficient; w is volume-average single scattering albedo, $\frac{\mu_r}{\mu_0+1} = \frac{\cos(\theta_r)}{\cos(\theta_i)+1}$; $p(\theta_p)$ is volume-average single-particle scattering function; θ_p is phase angle; B_S is the shadow-hiding opposition effect (SHOE)—part of the total opposition effect. B_{S0} is the amplitude of the SHOE effect, B_{C0} is the amplitude of the coherent backscattering opposition effect (CBOE)—the second part of the total opposition effect—and $H(x)$ is an approximation of the Ambartsumian–Chandrasekhar function, as described in Hapke (2012). It is helpful to clarify what some of these parameters mean physically.

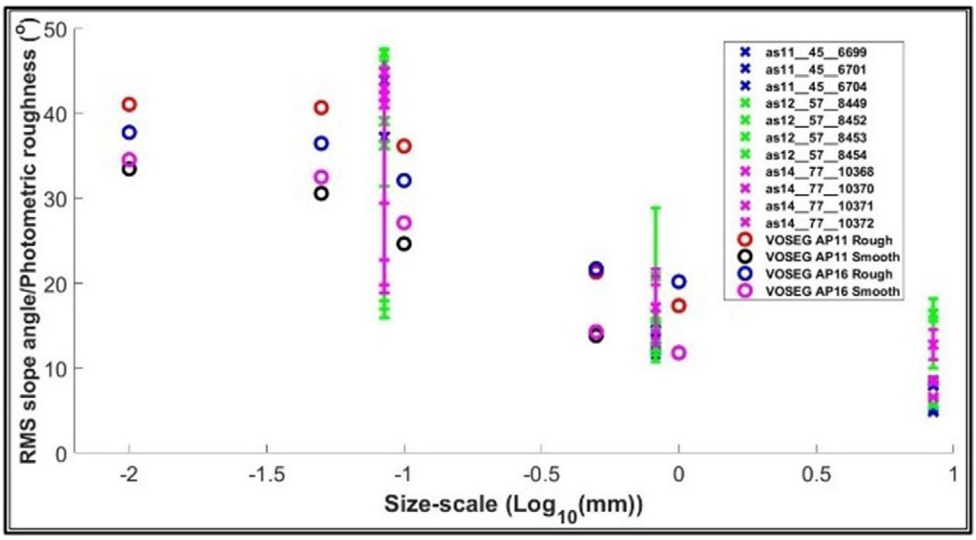

FIGURE 3. The RMS slope angle values measured for the Apollo 11 (10084) and Apollo 16 (68810) rough and smooth samples used in the VOSEG BRDF study across a range of size-scales (plotted on a $\log_{10}$ scale). Also, for comparison, showing the photometric roughness values determined in the Helfenstein and Shepard (1999) stereophotogrammetry study using images of the lunar surface taking during the Apollo 11, 12, and 14 missions. Apollo images named ASXX-YY-ZZZZ, where XX refers to the mission number and YY and ZZZZ refer to the specific image. Upper error bars for the Helfenstein and Shepard (1999) data for the lowest measured size-scale (85 mm) are not shown, as they reach up to ~78° RMS slope angle.

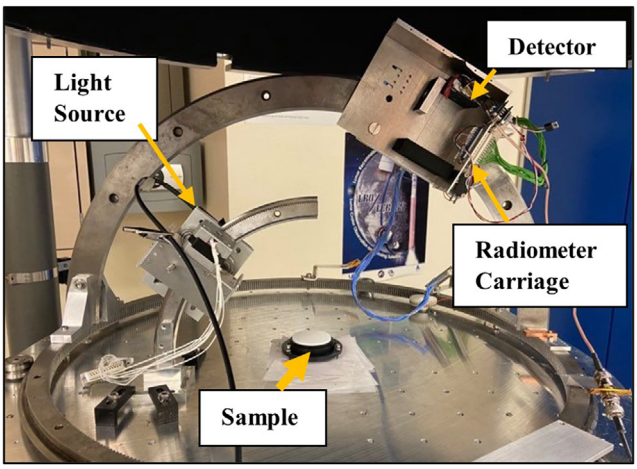

FIGURE 4. The Visible Oxford Space Environment Goniometer measuring White Spectralon®, with major parts labeled.

ω is the average particle single scattering albedo, which quantifies the efficiency of an average grain in scattering and absorbing light at a specific wavelength (Equation 3).

$$\omega = \frac{\sigma_{\text{sca}}}{\sigma_{\text{sca}} + \sigma_{\text{abs}}} \tag{3}$$

where σ_{sca} and σ_{abs} are the scattering and absorption coefficients, respectively. They quantify the fraction of light scattered or absorbed by a medium. Hence, $0 \leq \omega \leq 1$.

K is the porosity coefficient, a measure of how porosity affects transmission within a medium. For particle sizes $> \lambda$, it is related to the filling factor, φ (Equation 4):

$$K = \frac{-\ln\left(1-\left(1.209\phi^{\frac{2}{3}}\right)\right)}{\left(1.209\phi^{\frac{2}{3}}\right)} \tag{4}$$

$p(\theta_p)$ is the volume-average single-particle phase function, modeled as a Henyey–Greenstein (HG) function of one, two, or three terms. It can also be modeled as a Legendre polynomial, but HG is used here as it describes complex Mie scattering with equal accuracy to the Legendre polynomial, but with fewer parameters (McGuire & Hapke, 1995). The three-term HG function is defined in Hapke (2012) and contains the respective forward- and backscattering parameters, b and c.

In addition to porosity, the influence of surface roughness is included within the model in Hapke (1984) by multiplying $r(\theta_r, \theta_i, \theta_a)$ by a shadowing factor, $S(\theta_r, \theta_i, \theta_p)$, given in Equation (5), which is dependent on viewing angle, and the slope angle of the surface, $\overline{\theta}$:

$$S(\theta_r,\theta_i,\theta_a)=\frac{\mu_r}{\eta_r(\theta_r)}\frac{\mu_0}{\eta_{0r}(\theta_i)}\cdots \frac{\chi(\overline{\theta})}{1-f(\theta_p)+f(\theta_p)\chi(\overline{\theta})\left[\frac{\mu_0}{\eta_{0r}(\theta_i)}\right]} \quad (5)$$

where $f(\theta_p)=\exp\left(-2\tan\left(\frac{\theta_p}{2}\right)\right)$, $\chi(\overline{\theta})=\frac{1}{\left(1+\pi\tan^2(\overline{\theta})\right)^{1/2}}$, and $\eta_r(\theta_r)$ and $\eta_{0r}(\theta_i)$ are the effective cosines which appear within the shadowing factor—for θ_r and θ_i, respectively—as defined in Hapke (2012).

Reflectance, with surface roughness included, is thus described in Equation (6):

$$r_R(\theta_r,\theta_i,\theta_a)=r(\theta_r,\theta_i,\theta_a)S(\theta_r,\theta_i,\theta_a) \quad (6)$$

The nine free parameters within the Hapke BRDF model—ω, b, c, h_S, h_C, B_{S0}, B_{C0}, ϕ, $\overline{\theta}$—enable laboratory-measured (or remotely sensed) BRDFs to be related to the physical and compositional properties of a particulate surface; however, to deduce best fit values for three of them—that is, ω, b, and h_S—the six other parameters must be set, either using laboratory measurements or reasonable assumptions (Curtis, Warren, & Bowles, 2021a; Foote et al., 2020; Sato et al., 2014).

For the Hapke BRDF model fitting processes used on the laboratory data in this study, due to an inability to separate the SHOE and CBOE effects, B_{S0} and h_S are set as 1, and B_{C0} and h_C are set to 0, as in Sato et al. (2014) and Foote et al. (2020). The filling factor and slope angle values are set as the values determined by the surface profiling technique described above. Crucially, for the values reported in the abstract of this study, the laboratory measured RMS slope angle values determined for the 500 μm size scale are used, in accordance with the results of Part 3.2, which suggest that this is the most relevant size-scale for the BRDF. As in Sato et al. (2014), the backscattering parameter, c, is set in relation to b using the Hockey-stick relation, given in Equation (7):

$$c=3.29e^{-17.4b^2}-0.908 \quad (7)$$

Once six of the nine free parameters are set, as described above, the Hapke BRDF model can be fitted to the laboratory data using a least-squares Levenberg–Marquardt fitting function with three open parameters (MATLAB's *lsqcurvefit*) to determine best fit ω, b, and h_S values for the sample.

Values for Lambert Albedo, $A_L(\theta_r,\theta_i,\theta_a)$, Hemispheric Albedo, $A_H(\theta_r,\theta_i,\theta_a)$, and Albedo, $A(\theta_r,\theta_i,\theta_a)$ can then be derived from the measured BRDFs using Equations (8–10) (Shepard, 2017):

$$A_L(\theta_r,\theta_i,\theta_a)=\pi\frac{\mathrm{BRDF}(\theta_r,\theta_i,\theta_a)}{\cos(\theta_i)} \quad (8)$$

$$A_H(\theta_r,\theta_i,\theta_a)=\pi A_L(\theta_r,\theta_i,\theta_a)\cos(\theta_r) \quad (9)$$

$$A(\theta_r,\theta_i,\theta_a)=\pi A_H(\theta_r,\theta_i,\theta_a) \quad (10)$$

RESULTS

BRDF Measurements

Apollo 11

Figure 5 shows BRDF data measured by VOSEG in the principal plane, for the smooth Apollo 11, 10084 sample. Data at 15°, 30°, 45°, and 60° incidence angles are included, in addition to Hapke BRDF model best fit curves, calculated by fitting the model to the complete data set.

Figure 6 shows the equivalent BRDF data set measured in the principal plane for the rough Apollo 11, 10084 sample. Again, data at 15°, 30°, 45°, and 60° incidence angles is included, in addition to Hapke BRDF model best fit curves, calculated by fitting the model to the complete data set.

Figures S10–S13 show the differences between the two samples, by plotting ΔBRDF values for each incidence angle measurement set; calculated as the BRDF profile for the smooth sample minus the BRDF profile for the rough sample. For an interpretation of these differences, see the supplementary materials.

Apollo 16

Figure 7 shows BRDF data measured in the principal plane for the smooth Apollo 16, 68810 sample. The images are shown in the same way as for the 10084 BRDF plots. All 68810 measurements are for sample #1 in Table 1.

Figure 8 shows the equivalent BRDF data set measured in the principal plane for the rough Apollo 16, 68810 sample. Again, data at 15°, 30°, 45°, and 60° incidence angles are included, in addition to Hapke BRDF model best fit curves, calculated by fitting the model to the complete data set.

Figures S14–S17 show the differences between the two samples, by plotting ΔBRDF values for each incidence angle measurement set; calculated as the BRDF profile for the smooth sample minus the BRDF profile for the rough sample. For an interpretation of these differences, see the supplementary materials.

For BRDF data measured in the out-of-principal and diagonal planes, see the supplementary materials. Filling factors and RMS slope angles (at 500 μm) for each of the samples, measured with the Alicona 3D®, are as given in Table 1.

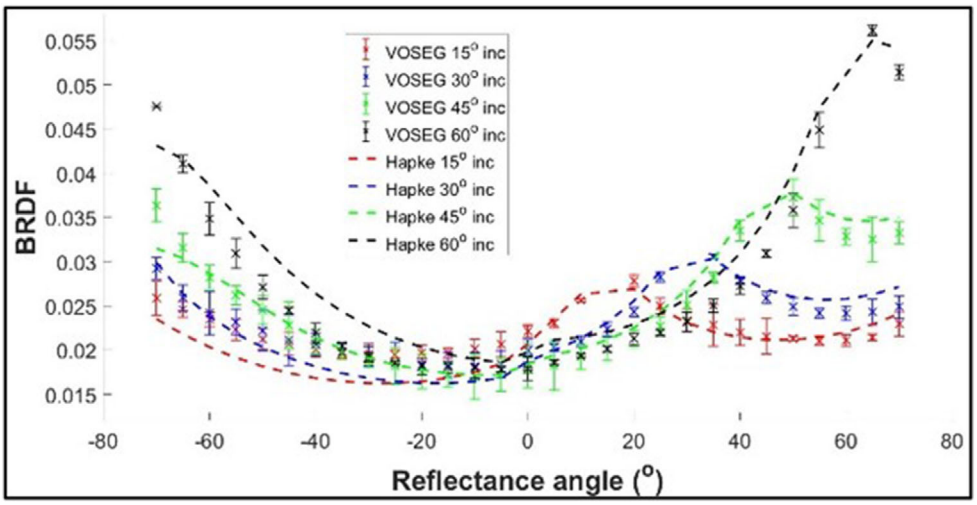

FIGURE 5. BRDFs measured by VOSEG, and fitted with the Hapke model over the complete data set, for the smooth Apollo 11, 10084 sample in the principal plane (i.e., azimuthal angle = 0/180°) at 15° (red), 30° (blue), 45° (green), and 60° (black) incidence angles. Positive θ_r values denote $\theta_a = 0°$, and negative θ_r values denote $\theta_a = 180°$.

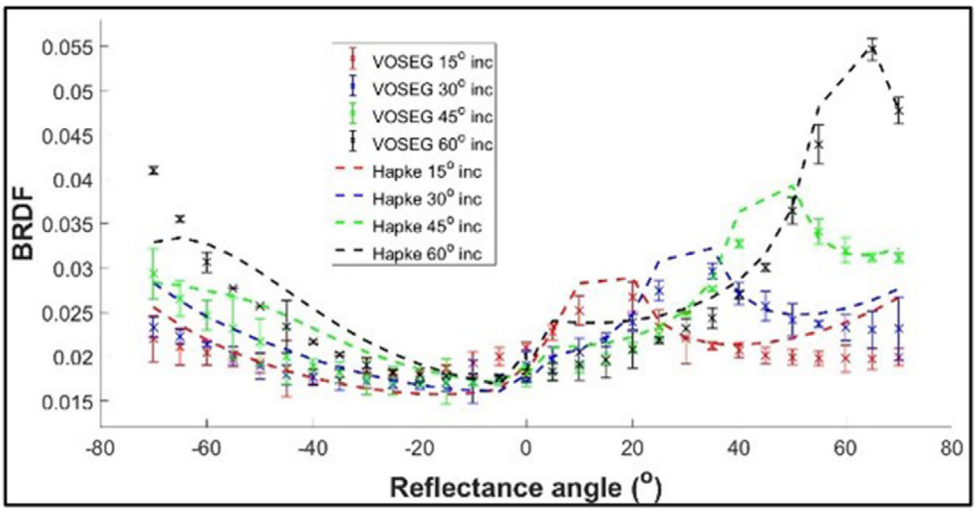

FIGURE 6. BRDFs measured by VOSEG, and fitted with the Hapke model over the complete data set, for the rough Apollo 11, 10084 sample in the principal plane (i.e., azimuthal angle = 0/180°) at 15° (red), 30° (blue), 45° (green), and 60° (black) incidence angles. Positive θ_r values denote $\theta_a = 0°$, and negative θ_r values denote $\theta_a = 180°$.

Deduction of Hapke Parameters and Further Constraining the Hapke Slope Angle Parameter

The constraint on the $\overline{\theta}$ size-scale given in Hapke (2012) is 100 μm to 1 km, due to the fact that $\overline{\theta}$ is expected to be affected by a convolution of all the scales within this range (e.g., by micro- and macro-scale roughness). For a given lunar regolith surface, $\overline{\theta}$ may be at least $\sim 5^{\circ} < \overline{\theta} < \sim 45^{\circ}$ across this range of size-scales, and therefore, any value determined for $\overline{\theta}$ is practically meaningless unless the size-scale is constrained (e.g., to within ~1–2 orders of magnitude, see Figure 3). Therefore, to constrain the most relevant size-scale of $\overline{\theta}$, this study fitted the Hapke model to the Apollo BRDF data with $\overline{\theta}$ set across 10–1000 μm size-scales, separately, using two fitting processes. Thus, the most relevant size-scale(s) for the BRDF could be deduced. The methodologies used for, and conclusions drawn from, the two Hapke fitting processes are described in the supplementary materials.

Hapke Model Complete Fitting Method Results

In general, the study shows that using $\overline{\theta}$ values at the three smallest size-scales (10, 50, and 100 μm) produces "poor" ($R^2 < 0.6$) fits to the data set, for all samples. In contrast to this, using $\overline{\theta}$ values at the two largest

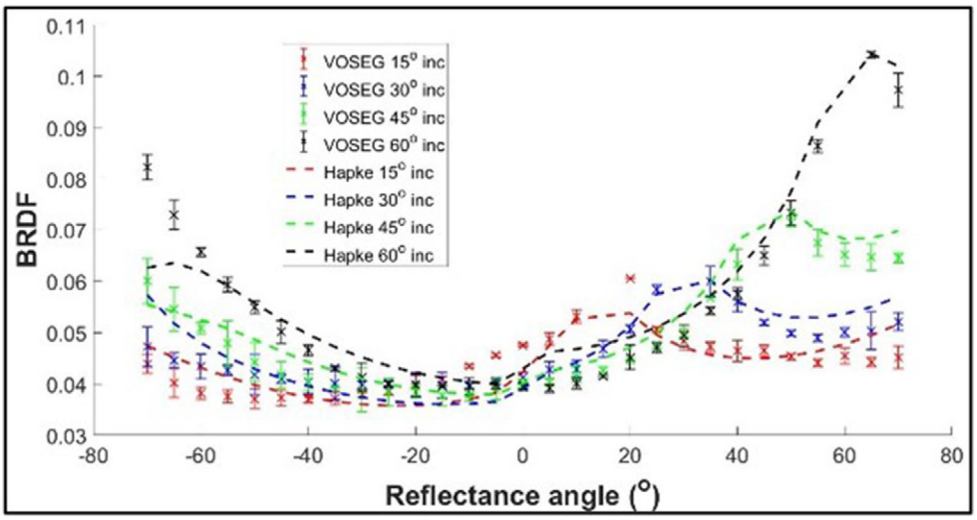

FIGURE 7. BRDFs measured by VOSEG, and fitted with the Hapke model over the complete data set, for the smooth Apollo 16, 68810 sample in the principal plane (i.e., azimuthal angle = 0/180°) at 15° (red), 30° (blue), 45° (green), and 60° (black) incidence angles. Positive θ_r values denote θ_a=0°, and negative θ_r values denote θ_a=180°.

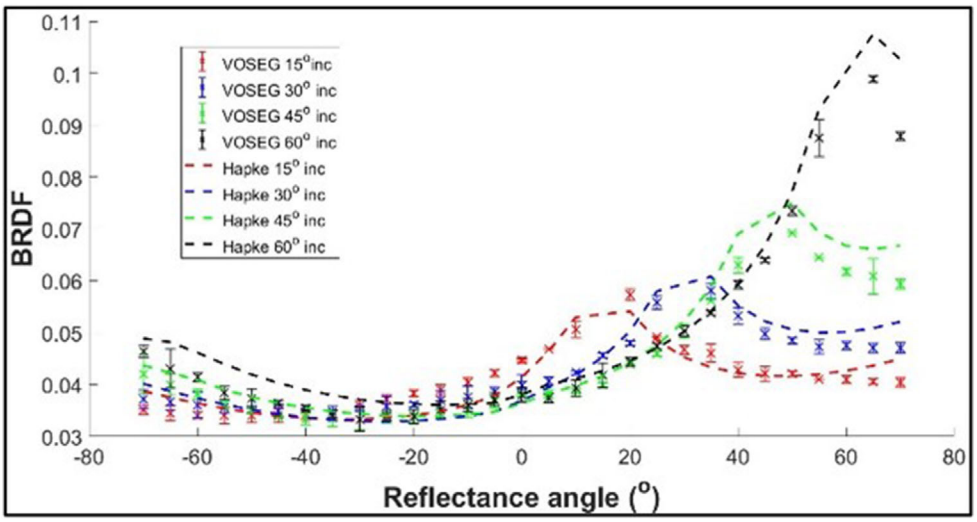

FIGURE 8. BRDFs measured by VOSEG, and fitted with the Hapke model over the complete data set, for the rough Apollo 16, 68810 sample in the principal plane (i.e., azimuthal angle = 0/180°) at 15° (red), 30° (blue), 45° (green), and 60° (black) incidence angles. Positive θ_r values denote $\theta_a = 0°$, and negative θ_r values denote $\theta_a = 180°$.

size-scales (500 and 1000 μm) generally produces "good" ($R^2 \geq 0.6$) fits, except for the marginally "poor" fit to the rough Apollo 16, 68810 data. For the complete fitting process over the Apollo 11 data, using $\overline{\theta}$ values at the 500 μm size-scale provides the best fits, for both rough and smooth samples. Contrastingly, when fitting over the Apollo 16 data, using $\overline{\theta}$ values at the 1000 μm size-scale provides the best fits, for both rough and smooth samples. However, fitting with $\overline{\theta}$ values at both these size-scales generally leads to "good" fits, with $R^2 \geq 0.6$ (with an exception at 500 μm for the rough Apollo 16 sample). Therefore, the appropriate "practical" size-scale of the Hapke slope angle parameter when fitting the Hapke BRDF model for the lunar regolith can be considered to be between 500 and 1000 μm. Considering the average particle diameter of the lunar regolith is on the order of ~100 μm, size-scales of a few times this value makes physical sense, because the shadows cast by lunar regolith particles (at the measured range of incidence angles) will be on the order of 10–500 μm (e.g., a 100 μm diameter particle will cast a 173 μm shadow at $\theta_i = 60°$). The $\overline{\theta}$ values measured at the 500 μm size-scale (which has the highest average R^2 value) are therefore used for the samples in this study.

The Sato et al. (2014) remote sensing study derives the single value of $\overline{\theta}$ it uses for the study (23.4°) by fitting the model to $1 \times 1°$ tile regions within an equatorial strip of the lunar surface (3° S to 3° N; 0–360° E) and averaging the best fit values. This value of $\overline{\theta}$ is higher than the values measured for the VOSEG Apollo samples at the 500 and 1000 μm size-scales. However, it is within 8% of the $\overline{\theta}$ values measured for the rough 10084 and 68810 samples, at 500 μm. This provides an initial indication that the regolith surface roughness profiles present on the lunar surface—as derived using remote sensing data—are similar to those of the rough 10084 and 68810 samples used in this study. The $\overline{\theta}$ values used in the Foote et al. (2020) study are 10.25° and 10.5° for the 68810 and 10084 samples, respectively. These values are within 15% of the $\overline{\theta}$ values measured for the smooth Apollo samples used in the VOSEG study, at the 1000 μm size-scale; thus, the study suggests the surface roughness profiles present in the lunar regolith are similar to those of the VOSEG study's smooth 10084 and 68810 samples; however, the samples used in the Foote et al.'s (2020) study were prepared using a similar method to the smooth samples in this study.

The h_S values deduced by the Sato et al. (2014) study are 0.050 ± 0.008 and 0.074 ± 0.009, for the mare and highlands regions, respectively. The h_S values deduced by the Foote et al.'s (2020) study for the two samples are both 0.011, and for the VOSEG study, the best fit h_S values when fitting with $\overline{\theta}$ values set at 500–1000 μm size-scales are 0.022 ± 0.006, 0.086 ± 0.007, 0.265 ± 0.023, and 0.252 ± 0.025, with an average of 0.165 ± 0.015 for the 10,084 samples; and 0.140 ± 0.012, 0.169 ± 0.016, 0.111 ± 0.011, and 0.080 ± 0.011 with an average of 0.125 ± 0.013 for the 68810 samples. Therefore, the VOSEG study deduces the highest h_S values, with those deduced by the Sato et al. (2014) study around a half to a third as high, and those deduced by the Foote et al.'s (2020) study around an eighth to a tenth as high. For the Sato et al. (2014) study, this may be explained by the fact the remote sensing data set did not contain data at low phase angles (<15°), and so there were insufficient data to accurately constrain the h_S parameter, but for the Foote et al.'s (2020) study, the minimum phase angle was 3°—compared to 5° for VOSEG—for the measured principal plane BRDF data, and so this cannot explain the one order of magnitude discrepancy between the deduced values. Therefore, this may also be due to differences in the semi-empirical simplifications performed within the two Hapke BRDF models.

With no information about the physical properties of the lunar surface measured in the Sato et al. (2014) study, φ is set to 0, and so $K = 1$. This should lead to higher w values than would be expected if measured values of φ were set, as is done within the model for the VOSEG study (in which φ = 0.4–0.6). The Foote et al.'s (2020) study does not specify whether it sets φ to be 0, or whether it uses values deduced for the samples, but varying φ between 0 and 0.6 can vary K by up to 46%, and—due to K and w serving similar functions within the model—setting φ to be 0 can lead to w values which are overestimated by up to ~46%. The w values deduced for the lunar mare and lunar highlands regions by the Sato et al. (2014) study are 0.201 ± 0.01 and 0.356 ± 0.01, respectively. The w values deduced for the Apollo 11 and Apollo 16 regolith samples in the Foote et al.'s (2020) study are 0.288 and 0.484, respectively. For the VOSEG study, when fitting with $\overline{\theta}$ values at the 500–1000 μm size-scales, the deduced w values are 0.385, 0.320, 0.143, and 0.127, with an average of 0.244 for the Apollo 11, 10084 samples; and 0.417, 0.378, 0.428, and 0.383, with an average of 0.402 for the Apollo 16, 68810 samples. Therefore, the VOSEG study deduces w values for the mare and highlands regolith which are ~21% and ~13% higher than those deduced by the Sato et al.' (2014) study, respectively; but w values which are ~18% and ~20% lower than those deduced by the Foote et al.'s (2020) study, respectively. If the Foote et al.'s (2020) study sets φ to be 0, this discrepancy could be explained by the accurately set φ values within the VOSEG study. The discrepancy between the Sato et al. (2014) and VOSEG studies cannot be explained by porosity, however, as the model set φ to be 0, and so $K = 1$. The lunar regolith surface is highly porous, and, considering the low surface gravity on the Moon, the porosities of the lunar regolith surfaces probed by the remote sensing study are likely to be higher still than those of the Apollo samples prepared in the laboratory. If the porosity of these remotely sensed regions was higher than for the VOSEG samples (and so φ was lower), and if Sato et al. (2014) ran the model with $K = 1$, instead of a more accurate, higher value (i.e., $K = 1.115$, from $\varphi = 0.3$), then this would reduce the w value further, thus increasing the discrepancy between the w values deduced by the two studies. Otherwise, the discrepancy may be caused by the various semi-empirical simplifications made within the version of the Hapke BRDF model used in the Sato et al. (2014) study, or the fact the Sato et al. (2014) model is run over all mare regions of the lunar surface, and not just for petrologies similar to those of the Apollo 11 regolith samples, which, as is typical for regolith samples, are more plagioclase- and pyroxene-rich than general mare surfaces. This is demonstrated in Greenhagen et al. (2020).

Setting $\overline{\theta}$ between the range of values used in the three studies, for example, 10.25–23.40°, will lead to variations in b, as the function attempts to accommodate for the change in curve shape by varying the amplitude of the forward- and backscattering terms. The b values derived for the mare regions of the Foote et al.'s (2020) and Sato et al. (2014) studies are 0.292 and

0.260 ± 0.010, respectively; and for the highlands regions of the two studies, they are 0.277 and 0.230 ± 0.010, respectively. The VOSEG study derives b values between 0.265 and 0.334 for the 10084 samples, when using $\overline{\theta}$ values at 500–1000 μm size-scales. For 68810, the VOSEG study derives b values of 0.117 and 0.089 for the smooth sample, and the function minimizes b for the rough sample (as so sets it to be 0.001). This suggests the model struggles to accommodate for the shape of the 68810 laboratory measured data, when fitting over the complete BRDF data set at once. The Foote et al.'s (2020) study did not have the same issue, as it only had to fit to principal plane and out-of-principal plane data. Therefore, the inclusion of BRDFs measured in the diagonal plane appears to disrupt the fitting function, for the 68810 data set.

These results are tabulated in Part A5.1 of the supplementary materials.

Hapke Model Split Fitting Method Results

Using the split fitting method, the average Hapke parameter values deduced by the study over the 500 μm and 1000 μm size-scales are as follows.

The average w values are determined as 0.281 ± 0.028 and 0.315 ± 0.021 for the 10084 smooth and rough samples, respectively, and 0.388 ± 0.057 and 0.485 ± 0.155 for the 68810 smooth and rough samples, respectively. Therefore, the w value determined for the 10084 samples is ~22% higher than for the complete fitting method, and hence, the value now agrees with the Foote et al.'s (2020) study, although it is further from the value determined for the mare in the Sato et al.' (2014) study. The w value determined for the 68810 samples using the split fitting method increased by ~9%, as compared to the complete fitting method. Therefore, this value is also now in agreement with the value determined by the Foote et al.'s (2020) study, although once again it has diverged further from the value determined for the highlands in the Sato et al. (2014) study.

The average b values are determined as 0.238 ± 0.008 and 0.261 ± 0.007 for the 10084 smooth and rough samples, respectively, and 0.063 ± 0.033 and 0.155 ± 0.183 for the 68810 smooth and rough samples, respectively. Hence, the b value determined for the 10084 sample has increased by ~213%, and the b value determined for the 68810 sample has increased by ~22%. This removes the discrepancy between the values determined by the VOSEG and Sato et al. (2014) studies (e.g., $b = 0.250 \pm 0.008$ [VOSEG] and $b = 0.260 \pm 0.010$ [Sato]), for the mare/10084 sample, and it brings the value to within ~13% of the value determined in the Foote et al.'s (2020) study ($b = 0.292$). For 68810, the average deduced b value has increased by ~22%, as compared to the complete fitting process, although this value is still a factor of 2.5–3 times lower than the values determined in the Sato et al. (2014) and Foote et al.'s (2020) studies. This may be due to inconsistencies in the functions used within the Hapke BRDF model, thus motivating a standardized modeling approach.

The average h_S values are determined to be 0.032 ± 0.006 and 0.039 ± 0.005 for the 10084 smooth and rough samples, respectively, and 0.221 ± 0.149 and 0.135 ± 0.148 for the 68810 smooth and rough samples, respectively. Importantly, the split fitting method leads to best fit h_S values which are closer to the values determined in the Sato et al. (2014) and Foote et al.'s (2020) studies, in particular for the rough 10084 sample, which is in agreement with the Sato et al. (2014) mare value. Although the deduced VOSEG 10084 values are closer to the Foote et al.'s (2020) study than for the complete fitting process values, they are still higher than this study's values by approximately a factor of 3. While the average deduced h_S value for the 10084 sample has decreased by ~80% for the 10084 sample—meaning the value is closer to the two remote sensing studies—the average deduced h_S value for the 68810 sample has increased by ~42%, meaning the discrepancy has also increased between the VOSEG study and the two remote sensing studies. Again, this may be due to inconsistencies in the functions used within the Hapke BRDF model.

These results are tabulated in Part A5.2 of the supplementary materials.

Derived Hemispheric Albedo Functions

As in the Foote et al.'s (2020) study, VOSEG's BRDF measurements of the rough and smooth 10084 and 68810 samples were used to derive hemispheric albedo functions, but without first fitting the Hapke BRDF model to the data. The hemispheric albedo values calculated in this study, at each measured incidence angle, are given in Table 2, alongside those derived using the Foote et al.'s (2020) data.

From the data given in Table 2, hemispheric albedo functions can be approximated, using a cosine relation, for θ_i=0–90°, as shown in Figure 9.

Figure 9 demonstrates how hemispheric albedo functions derived from laboratory measurements of the Apollo regolith samples are considerably flatter than those assumed in previous thermal models (Hayne et al., 2017; Keihm, 1984; Vasavada et al., 1999). The shapes of the derived curves are generally concordant with those derived in Foote et al. (2020); however, the 68810 sample has a generally higher hemispheric albedo (particularly at $\theta_i \leq 30°$) than was assumed in Foote et al. (2020) for highlands regolith.

TABLE 2. Hemispheric albedo values derived from the VOSEG and BUG BRDF measurements of the Apollo 11, 10084 and Apollo 16, 68810 regolith samples. No errors were reported for the BUG data.

	Hemispheric albedo			
	θ_i			
Sample/study	15°	30°	45°	60°
Rough 10084	0.1262 ± 0.0059	0.1252 ± 0.0054	0.1272 ± 0.0066	0.1365 ± 0.0042
Smooth 10084	0.1330 ± 0.0071	0.1334 ± 0.0070	0.1329 ± 0.0086	0.1413 ± 0.0053
Rough 68810	0.2557 ± 0.0066	0.2543 ± 0.0072	0.2565 ± 0.0083	0.2885 ± 0.0089
Smooth 68810	0.2729 ± 0.0102	0.2702 ± 0.0129	0.2822 ± 0.0143	0.3184 ± 0.0136
BUG—10084	0.1340	0.1251	0.1152	0.1000
BUG—68810	0.2817	0.2598	0.2351	0.2787

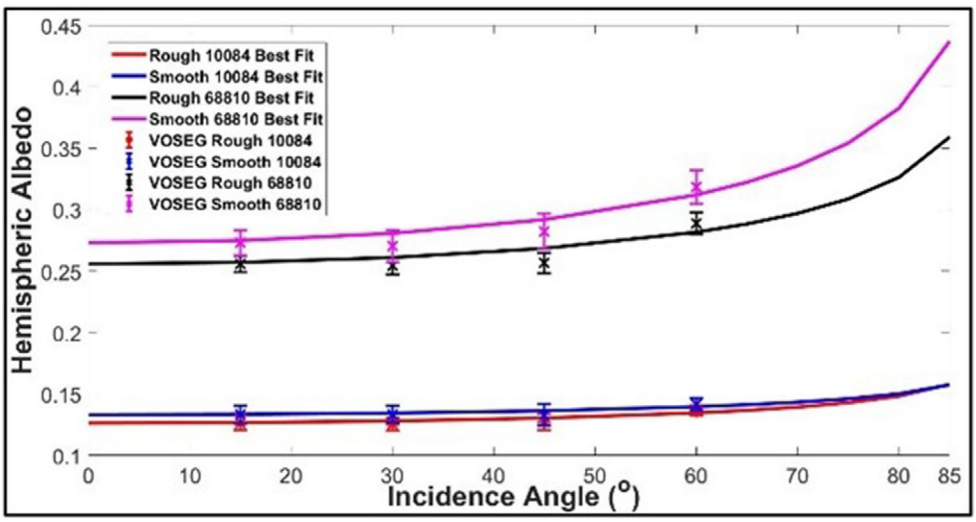

FIGURE 9. Hemispheric albedo functions derived from VOSEG's BRDF measurements of the Apollo 11, 10084 and Apollo 16, 68810 samples, which were measured at $\theta_i = 15°$, 30°, 45°, and 60°. The values at $\theta_i = 0°$ are assumed to be equal to those at $\theta_i = 15°$ to enable approximations to be determined with albedo $= b/(\cos(\text{inc})^n)$, where b is the albedo value at $\theta_i = 15°$ for each sample, and best fit n values are: $n = 0.0916$ for Rough 10084, $n = 0.0688$ for Smooth 10084, $n = 0.1391$ for Rough 68810 and $n = 0.1928$ for Smooth 68810. $\theta_i > 85°$ are not shown, as here the curve is asymptotic.

CONCLUSIONS AND FUTURE WORK

This study identified the need for laboratory measured visible scattering functions of lunar regolith samples characterized in terms of surface properties, in light of recent photometry studies (Foote et al., 2020; Hapke, 2012; Shepard & Helfenstein, 2007), and hence, it explored the utility of such a laboratory data set, in terms of testing and constraining key terms within the Hapke BRDF model. The main conclusions of the study are as follows:

- A suite of BRDFs was measured for well-characterized, "smooth" and "rough" representative (mare and highlands) Apollo regolith samples.
- The surface profiling process performed on the samples enabled two of the free parameters within the Hapke BRDF model to be set, allowing deductions to be made for three of the other key parameters, w, b and h_S.
- To determine the relevant size-scale of $\overline{\theta}$, the Hapke BRDF model was fitted to the VOSEG data using measured $\overline{\theta}$ values at each of the size-scales, between 10 and 1000 μm. A general trend was deduced and 500–1000 μm was determined to be the practical size-scale range most well represented by $\overline{\theta}$.
- The Hapke BRDF model was fitted to the VOSEG Apollo sample BRDF data (using $\overline{\theta}$ values at 500–1000 μm) with w, b, and h_S set as the three open parameters. w, b, and h_S values were determined for each sample. These values were then compared to the relevant values determined in Sato et al. (2014) and Foote et al. (2020). This was done for both complete and split fitting methods and the results were compared.
- Finally, VOSEG's laboratory measured BRDFs for the rough 10084 and 68810 samples were used to derive hemispheric albedo functions which could be used to set more realistic scattering function inputs within thermal models, such as the O3DTM.

Many of the results of this project are dependent upon the physicality of the Hapke BRDF model, which has been updated multiple times since its conception. In terms of further improving the utility of the model, a future study is needed in which polarizers are used to distinguish between the effects of the SHOE and CBOE contributions to the total opposition effect (Hapke, 2021). This would lead to more accurately deduced h_S values.

In light of this study's investigation into the methods used when fitting the Hapke BRDF model to laboratory BRDF data, it may prove useful to compare the best fit Hapke parameters outputted by this study to those outputted by a Bayesian statistics fitting approach, such as the one detailed in Belgacem et al. (2018).

Furthermore, it may be possible to compare the BRDFs measured for the Apollo regolith samples in this study to those measured by Diviner's off-nadir extended mission campaign for various targets on the lunar surface. Hence, it may be possible (1) to compare the scattering behavior of each target to both mare-like and highlands-like regolith, thus enabling deductions to be made about these regions of the lunar surface; and (2) to discern whether regions with similar regolith petrologies, but different latitudes, exhibit higher or lower albedo scattering functions, potentially due to variations in porosity.

In addition, now that visible-λ scattering functions can be set within 3-D thermal model using laboratory measurements—as opposed to setting them so that the model best matches Diviner—it may be possible to study whether the lunar surface exhibits a latitude dependence on porosity, as suggested in Metzger et al. (2018).

Finally, BRDF measurements such as those detailed in this study may help to shed light on other key unanswered questions in lunar science, such as whether the Reiner Gamma lunar swirls are associated with physical differences (as opposed to compositional differences) between bright and dark "lanes" on the lunar surface, or they may be used to improve our understanding of how lunar surface operations and rocket landings affect the physical structure of the regolith present at mission landing sites.

This project has demonstrated how laboratory-measured lunar regolith scattering functions may be used to further constrain key parameters within the Hapke BRDF model. Yet, the Moon is not the only airless body of interest in the solar system, and studies similar to this one could also be performed for Mercury, asteroids, and comets. Although no samples are yet to be returned from Mercury, the production of simulant samples is continuously improving, and much will be learnt about Mercury's surface from the measurements taken by Bepicolombo (Benkhoff et al., 2010). For asteroids and comets, recent successful sample retrieval missions may enable photometric measurements to be made for samples with known locations of origin (Lauretta et al., 2024); and meteorites collected on Earth soon after impact may also provide samples which can be measured in the laboratory to produce photometric data sets similar to those of the Apollo samples (King et al., 2022).

Acknowledgments—All authors would like to acknowledge the financial support of the Royal Astronomical Society (RAS) and the Scientific Technology Facilities Council (STFC). The authors would like to thank the Curation and Analysis Team for Extraterrestrial Materials (CAPTEM) for the Apollo samples, Dr. Kalin Dragnevski and Robert Spry for assistance with the Alicona 3D® measurements, and Professor Michael Shepard for his guidance regarding the VOSEG setup.

Data Availability Statement—The BRDF and Apollo sample surface profile data sets are available in the Oxford Research Archive or can be made available by the author upon reasonable request.

Editorial Handling—Dr. Edward Anthony Cloutis

REFERENCES

Belgacem, I., Schmidt, F., and Jonniaux, G. 2018. Estimation of Hapke Parameters on Selected Areas of Europa Using a Bayesian Approach. *49th Lunar and Planetary Science Conference*, abstract 2083.

Benkhoff, J., van Casteren, J., Hayakawa, H., Fujimoto, M., Laakso, H., Novara, M., Ferri, P., Middleton, H. R., and Ziethe, R. 2010. BepiColombo-Comprehensive Exploration of Mercury: Mission Overview and Science Goals. *Planetary and Space Science* 58: 2–20.

Biggar, S. F., Thome, K. J., and Wisniewski, W. 2003. Vicarious Radiometric Calibration of EO-1 Sensors by Reference to High-Reflectance Ground Targets. *IEEE Transactions on Geoscience and Remote Sensing* 41: 6–1179.

Curtis, R. J., Bates, H. C., Warren, T. J., Shirley, K. A., Brown, E. C., King, A. J., and Bowles, N. E. 2023. Bidirectional Reflectance Distribution Function Measurements of the Winchcombe Meteorite Using the Visible Oxford Space Environment Goniometer. *Meteoritics & Planetary Science* 59: 1029–42.

Curtis, R. J., Warren, T. J., and Bowles, N. E. 2021a. LPSC Abstract #1056: Measuring and Interpreting Bidirectional Reflectance Distribution Functions for Apollo Lunar Regolith Samples Using the Visible Oxford Space Environment Goniometer. *52nd Lunar and Planetary Science Conference*, abstract 2548, pp. 16–17.

Curtis, R. J., Warren, T. J., and Bowles, N. E. 2021b. Updates to the Oxford Space Environment Goniometer to Measure Visible Wavelength Bidirectional Reflectance Distribution Functions in Ambient Conditions. *Review of Scientific Instruments* 92: 034504.

Foote, E., Paige, D. A., Shepard, M. K., Johnson, J. R., Biggar, S. F., Greenhagen, B. T., et al. 2010. Apollo 11

and 16 Soil Bi-Directional Solar Reflectance Measurements, Models and LRO Diviner Observations. *AGU Fall Meeting Abstracts* 53A: 1499.
Foote, E., Paige, D. A., Shepard, M. K., Johnson, J. R., and Biggar, S. 2020. The Bidirectional and Directional Hemispheric Reflectance of Apollo 11 and 16 Soils: Laboratory and Diviner Measurements. *Icarus* 336: 113456.
Greenhagen, B. T., Wagoner, C. M., Yasanayake, C. N., Donaldson Hanna, K. L., Bowles, N. E., and Lucey, P. G. 2020. Using Mineral Mixtures Across the Lunar Mineralogy Ternary to Interpret LRO Diviner and Future Thermal Infrared Datasets, 51st Lunar and Planetary Science Conference, No. 2326.
Gunderson, K., Thomas, N., and Whitby, J. A. 2006. First Measurements with the Physikalisches Institut Radiometric Experiment (PHIRE). *Planetary and Space Science* 54: 1046–56.
Hapke, B. 1981. Bidirectional Reflectance Spectroscopy: 1. Theory. *Journal of Geophysical Research: Solid Earth* 86: 3039–54.
Hapke, B. 1984. Bidirectional Reflectance Spectroscopy. 3. Correction for Macroscopic Roughness. *Icarus* 59: 49–51.
Hapke, B. 1986. Bidirectional Reflectance Spectroscopy. 4. The Extinction Coefficient and the Opposition Effect. *Icarus* 67: 264–280.
Hapke, B. 2002. Bidirectional Reflectance Spectroscopy. 5. The Coherent Backscatter Opposition Effect and Anisotropic Scattering. *Icarus* 157: 523–534.
Hapke, B. 2008. Bidirectional Reflectance Spectroscopy. 6. Effects of Porosity. *Icarus* 195: 918–926.
Hapke, B. 2012. Bidirectional Reflectance Spectroscopy 7. *Icarus* 221: 1079–83.
Hapke, B. 2021. Bidirectional Reflectance Spectroscopy 8. The Angular Width of the Opposition Effect in Regolith-like Media. *Icarus* 354: 114105.
Hapke, B., Nelson, R., and Smythe, W. 1998. The Opposition Effect of the Moon: Coherent Backscatter and Shadow Hiding. *Icarus* 133: 89–97.
Hayne, P. O., Bandfield, J. L., Siegler, M. A., Vasavada, A. R., Ghent, R. R., Williams, J. P., Greenhagen, B. T., et al. 2017. Global Regolith Thermophysical Properties of the Moon from the Diviner Lunar Radiometer Experiment. *Journal of Geophysical Research: Planets* 122: 2371–2400.
Helfenstein, P., and Shepard, M. K. 1999. Submillimeter-Scale Topography of the Lunar Regolith. *Icarus* 141: 107–131.
Johnson, J. 2008. Spectrogoniometric Measurements and Models of Lunar Analog Soils. *39th Lunar and Planetary Science Conference*, abstract 1391.
Keihm, S. J. 1984. Interpretation of the Lunar Microwave Brightness Temperature Spectrum: Feasibility of Orbital Heat Flow Mapping. *Icarus* 60: 568–589.
King, A. J., Daly, L., Rowe, J., Joy, K. H., Greenwood, R. C., Devillepoix, H. A. R., Suttle, M. D., et al. 2022. The Winchcombe Meteorite, a Unique and Pristine Witness from the Outer Solar System. *Science Advances* 8: 1–17.
King, O., Warren, T., Bowles, N. E., Sefton-Nash, E., and Fisackerly, R. T. 2019. The Oxford 3D Thermophysical Model with Application to PROSPECT_Luna 27 Study Landing Sites. *Planetary and Space Science* 182: 104790.
Labsphere. 2017. Spectralon® Diffuse Reflectance Standards Datasheet, pp. 1–4.
Lauretta, D. S., Connolly, H. C., Jr., Aebersold, J. E., Alexander, C. M. O.'D., Ballouz, R. L., Barnes, J. J., Bates, H. C., et al. 2024. Asteroid (101955) Bennu in the Laboratory: Properties of the Sample Collected by OSIRIS-REx. *Meteoritics & Planetary Science* MAPS-4104: 1–34.
McGuire, A. F., and Hapke, B. W. 1995. An Experimental Study of Light Scattering by Large, Irregular Particles. *Icarus* 113: 134–155.
Metzger, P., Anderson, S., and Colaprete, A. 2018. Experiments Indicate Regolith Is Looser in the Lunar Polar Regions than at the Lunar Landing Sites Earth and Space 2018: Engineering for Extreme Environments, pp. 79–85.
Meyer, C. 2009. 10084, Bulk Soil (<1mm), 3,830 grams. Lunar Sample Compendium.
Morris, R. V. 1983. Handbook of Lunar Soils: Part I: Apollo 11-15.
Potin, S., Brissaud, O., Beck, P., Schmitt, B., Magnard, Y., Correia, J. J., Rabou, P., and Jocou, L. 2018. SHADOWS: A Spectro-Gonio Radiometer for Bidirectional Reflectance Studies of Dark Meteorites and Terrestrial Analogs: Design, Calibrations, and Performances on Challenging Surfaces. *Applied Optics* 57: 8279–96.
Rozitis, B., and Green, S. F. 2011. Directional Characteristics of Thermal-Infrared Beaming from Atmosphereless Planetary Surfaces—A New Thermophysical Model. *Monthly Notices of the Royal Astronomical Society* 415: 2042–62.
Sato, H., Robinson, M. S., Hapke, B., Denevi, B. W., and Boyd, A. K. 2014. Resolved Hapke Parameter Maps of the Moon. *Journal of Geophysical Research, E: Planets* 119: 1775–1805.
Shepard, M. K. 2017. *Introduction to Planetary Photometry*. Cambridge, UK: Cambridge University Press.
Shepard, M. K., and Helfenstein, P. 2007. A Test of the Hapke Photometric Model. *Journal of Geophysical Research, E: Planets* 112: E3.
Vasavada, A. R., Paige, D. A., and Wood, S. E. 1999. Near-Surface Temperatures on Mercury and the Moon and the Stability of Polar Ice Deposits. *Icarus* 141: 179–193.
Yoldi, Z., Pommerol, A., Jost, B., Poch, O., Gouman, J., and Thomas, N. 2015. VIS-NIR Reflectance of Water Ice/Regolith Analogue Mixtures and Implications for the Detectability of Ice Mixed within Planetary Regoliths. *Geophysical Research Letters* 42: 6205–12.

SUPPORTING INFORMATION

Additional supporting information may be found in the online version of this article.

Data S1. Supplmentary Materials include: 1) Sample preparation repeatability data, 2) a description of surface profiling process used in this study, 3) Bidirectional Reflectance Distribution Function (BRDF) data for the Apollo 11 (10084) and Apollo 16 (68810) samples measured in this study, and 4) data concerning the Hapke model fitting methodologies used in this study.